Journal of Sciences, Islamic Republic of Iran 36(2): 127 - 142 (2025) http://jsciences.ut.ac.ir
University of Tehran, ISSN 1016-1104

Theoretical Study of the Encapsulation of the Anticancer Drug of Letrozole: DFT/TD-DFT and Spectroscopic Studies

N. Masnabadi[1]*, S. Masoudi[2], S. Rahbari[2]

[1] *Department of Chemistry, Ro. C., Islamic Azad University, Roudehen, Islamic Republic of Iran*

[2] *Department of Chemistry, CT. C., Islamic Azad University, Tehran, Islamic Republic of Iran*

Received: 1 September 2025 / Revised: 3 December 2025 / Accepted: 30 May 2026

Abstract

The DFT description and comparison of the loading of Letrozole (LTZ) on boron nitride (AlNNT) and aluminum nitride (BNNT) nanotubes were studied herein. The results of the thermochemical parameters indicate that LTZ with AlNNT nanotube would be a more spontaneous and exothermic process in comparison with that of BNNT. The study included electron delocalization effects, stereoelectronic interaction, steric repulsion effects, electronic properties, and reactivity of LTZ on the AlNNT nanotube using DFT B3LYP/6-31G* level of theory. The UV-Vis absorption analysis and the IR spectrum were used to ascertain the changes that take place on adsorption of LTZ onto AlNNT. The molecular orbital distribution was further assessed to monitor electronic structure changes, adsorption energies (E_{ad}), and electrical conductivity during the adsorption process on both substrates. The NBO analysis of the LTZ-AlNNT complex shows that the highest resonance energy is provided due to the instability of electrons of LP (1)N73→ BD*(2)N75-C85 (51.96 kcal.mol-1), which in turn signifies that there is electron transfer from the LTZ drug in the LTZ-AlNNT complex. This in the UV-Vis spectrum corroborated by the drug adsorption-related wavelength change from 226.7 nm to 254.3 nm on the AlNNT demonstrates bathochromic shift.We hope that this study can aid in modeling and designing a suitable adsorbent for drug delivery based on its findings. Thus, electronic, thermochemical, and structural properties of LTZ drug complexes with the nanotubes AlNNT and BNNT were elucidated with a combination of DFT calculations and graphical analysis of the non-covalent interactions index (NCI) analysis.

Keywords: Adsorption energy; Aluminum nitride nanocarrier; Density functional theory (DFT); Letrozole.

Introduction

Nanoloading-based delivery systems have considerably affected cancer therapy. Advancements in nanotechnology and intelligent drug delivery present new and innovative ideas for nanocarriers that would open new avenues in the rehabilitation of cancer patients. Nanotechnology in the drug delivery system has created an active effect on selective recognition of body cells, targeted drug release, and overcoming chemotherapy limitations. Meanwhile, it has organized nanocarriers into appropriate groups for the delivery of anticancer drugs by a simple production process, biodegradability, and biocompatibility. Encapsulation refers to the new

[1] Corresponding Author: Tel: +98 9124493793; Email: na.masnabadi@iau.ac.ir; nasmasnabadi@gmail.com

technology concerned with packing solid, liquid or gaseous substances in microscopic capsules having the common factor of being in suspension in water and setting the conditions for control of release of the contents. This process is concerned with encasing food components, enzymes, cells, and other items in some small coating. With the increasing use of this technique, the materials contained in the coating are protected from moisture, heat, or other environmental conditions (1). Nanotubes are capable of piercing into the cell membrane without damaging it because they have sharp needle-like tips. So the drug can be encapsulated in the nanotube and remain safe as it passes through the body, liberating the drug from the nanotube after reaching the effective site with the destruction of the encapsulating material. Therefore, the drug should be contained in the nanotube in relation to its diameter and length (2, 3).

Carbon nanotubes have the possibility of specific bonding with cell receptor and intracellular target molecules that form the basis of considering these nanotubes for cancer therapy (4). The reports reveal entry of nanotubes into cells in the vertical direction via endocytosis (5). Boron nitride nanotubes possess more stable chemical properties as compared to carbon nanotubes, i.e. better resistance to oxidation at elevated temperatures. A few boron nitride nanotubes are perfect nanocrystalline structures, thus withstanding high temperatures (up to 900 degrees Celsius). In contrast, carbon nanotubes get oxidized in air (up to 400 degrees Celsius) (6). Therefore, one can state that boron nitride nanotubes could be used for the making of composites (7). Mention may also be made for the fact that boron nitride nanotubes are biodegradable and non-toxic materials permitting their use as nanocarriers in nanomedicine. Furthermore, they can better therapeutically action of the drug in comparison with other drug delivery systems by prolonged half-life or improving solubility for water-soluble drugs or controlling drug release and toxicity reduction of the drugs themselves while minimizing the possibility of a toxicity via superior accessibility of the nano-drugs to the diseased tissues, such as tumors. These are some of the other advantages of born nitride nanocarriers. By increasing the concentration of the drug within the diseased area and decreasing concentration inside the rest of the body, not only is the treatment made more effective, but also the chemical toxicity is reduced (8). For example, Yang et al. showed the interaction of Purinetol drug with B24N24 nanocages using DFT calculations and presented a purinetol nano sensor in this study. They also found that the electrical conductivity of the nanocages is raised quite significantly due to the interaction of the drug with the nanocages. Using the UV-Vis spectrum, the researchers in the present study demonstrated that the drug's wavelength transitions are shifted to a longer wavelength than drugs in the nanocage mixture. Thus, red shift is caused by the proximity of the purinetol drug to the nanocages (9). A similar study by Khalifi and colleagues demonstrated that the absorption of isofamide drug into the substrate, as well as within the nanotubes, can happen spontaneously within the inner wall of the nanotube (10).

Shakerzadeh and Nourizadeh, in another study, investigated anticancer drugs' reaction with boron nitride nanotubes and aluminum-doped boron nitride nanotubes. It was found that drug adsorption on the aluminum atom has been performed well, and further results indicate that aluminum doped boron nitride nanotubes constitute suitable nanocarrier systems for drug (11). Therefore, the study aims to investigate the interaction of the drug LTZ (C17H11N5) with Boron Nitride and Aluminum Nitride nanotubes using DFT quantum mechanics calculations at B3LYP/6-31G* for theoretical levels-the idea of which will Check: Using quantum mechanical computations based on density functional theory at the B3LYP/6-31G* level, the optimum arrangement of LTZ drug on a nanotube substrate with minimum energy and maximum stability was calculated. Using density functional theory-based quantum mechanical calculations at B3LYP/6-31G*, it has been compared for the physical adsorption and encapsulation of LTZ drug in the presence of born nitride and aluminum nitride nanotubes. From the non-bonding interaction of LTZ drug with boron nitride and aluminum nitride nanotubes, which of the two nanotubes is preferable to encapsulate LTZ drug and which of the two might be more amenable to smart drug delivery?

Materials and Methods

A single-walled armchair BNNT and AlNNT carbon nanotubes (6, 6) of 6 A˚ in length were used in the present study to evaluate the comparative improvement of efficiency and reduction of adverse effects of LTZ. Structures were erected and optimized according to the methodology of B3LYP (DFT) and the basis set 6-31G* method using Gaussian 09 (Figure 1) (12-15). The level of resilience in the electronic structure of the drug due to the interaction with single-walled BNNT and AlNNT nanotubes has been established through scanning bond angles and bond distances using the program, Gauss View. The frequencies were calculated for thermodynamic functions for both the structures of LTZ drug, BNNT, AlNNT nanotubes, and stable mixtures in gas phase with B3LYP/6-31G*, conducted in terms of thermodynamics. The study of molecular orbital interactions and density of states diagrams were carried

Figure 1. Optimized structures of LTZ drug, BNNT and AlNNT nanocarriers

out at the B3LYP/6-31G* level for the compounds in question using NBO analysis (16-19). The present research analyzed the factors related to the chemical behavior of the researched structures, including HOMO and LUMO energies, energy gap (Eg), and dipole moment. Thermochemical parameters, such as enthalpy of formation, Gibbs free energy of formation, and molecular and thermal energies for the optimized structures, were calculated and analyzed. The main motivations of the current investigation were to theoretically assess the controlled drug delivery by the complex BNNT-LTZ and AlNNT-LTZ. The assessment of the electronic properties, molecular electrostatic potentials, ultraviolet-visible (UV-Vis) spectra, absorption energy, and densities of states (DOS) of the systems was performed. It also served to analyze the character of the interactions.

Results and Discussion

Optimization and adsorption energy

The LTZ drug and single-walled armchair boron nitride and aluminum nitride nanocarriers (6,6) of length 6 A˚ were optimized by B3LYP/6-31G* in the gas phase under standard conditions. The LTZ drug was then attached in different orientations to boron nitride and aluminum nitride nanotubes with the semi-empirical method PM3. Among the orientations considered (Table 1), the BN-LTZ 2 and AlNNT-LTZ structures comprise the most stable drug-nanotube combinations with minimal energy; in the further study, the stable electronic structures of the BNNT-LTZ and AlNNT-LTZ obtained from the interaction of the drug with BNNT and AlNNT nanotubes were optimized using density functional theory (DFT) calculations based on the B3LYP method with the 6-31G* basis set (Figure 1 and Tables 1-2).

Results; size: 12; Normal, Subtitles in the text can be ordered numerically. Table 3 contains the electron energy, adsorption energy, and interaction energy values of LTZ in relation to the two types of nanotubes, BNNT and AlNNT. The energy optimization values of the LTZ

Table 1. Optimized structures of LTZ-BNNT and AlNNT (6, 6) drug mixtures in different directions with pm3 calculation method.

Abbreviation symbol	Structure
BN-LTZ 1	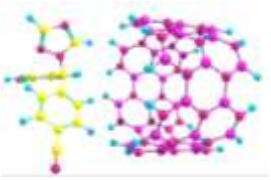
BN-LTZ 2	
BN-LTZ 3	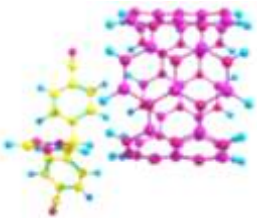
AlN-LTZ 1	
AlN-LTZ 2	
AlN-LTZ 3	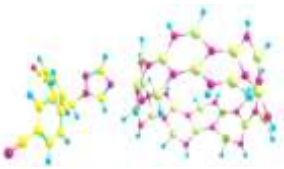

Table 2. Calculated energy values in the adsorption of LTZ by BNNT and AlNNT nanotubes from different directions.

		SCF done energy at pm3	
BN-LTZ	BN-LTZ 1		-2.2126964
	BN-LTZ 2	Optimization energy ($kcal.mol^{-1}$)	-2.2208584
	BN-LTZ 3		-2.2132194
AlN-LTZ			
	AlN-LTZ 1		-0.2658103
	AlN-LTZ 3		-0.2810053
	AlN-LTZ 3		-0.2628811

Table 3. Values of thermodynamic functions resulted from frequency calculations for LTZ drug, BNNT nanotube, and LTZ/BNNT mixture in gas phase.

Compounds	B3LYP/6-31G*		
	LTZ	**BNNT**	**LTZ/BNNT Mix**

drug, BNNT, and the LTZ-BNNT mixture have been obtained at the B3LYP/6-31G* level and are recorded as 928.146439, 2405.716746, and 3333.858862 Hartrees, respectively. The results indicate that this drug, LTZ, becomes more stable while entrapped within the BNNT nanotube than when this drug is outside the nanotube. The energies of adsorption of the LTZ drug onto an AlNNT nanotube substrate are respectively -7149.177691 and -8077.327137 Hartree, evaluated using the B3LYP/6-31G* method (Table 4). In this regard, the results point to the ability of AlNNT nanotube, like BNNT nanotube, in stabilizing LTZ. Thus, from the adsorption energy obtained, the more stable placement of LTZ drug on BNNT nanotube substrate can be compared with that placement of LTZ drug on AlNNT nanotube substrate. The amount of drug adsorption on the substrate of BNNT and AlNNT nanotubes can, therefore, be investigated by the followed relations 1 to 4.

$\Delta G=G(\text{drug nanotube-})–(G(\text{drug}) + G(\text{nanotube}))$ (1)

$\Delta H=H(\text{-drug nanotube})–(H(\text{drug}) + H(\text{nanotube}))$ (2)

$\Delta S=S(\text{drug-nanotube})–(S(\text{drug})+ S(\text{nanotube}))$ (3)

$\Delta E=E(\text{drug - nanotube})– (E(\text{drug}) + E(\text{nanotube}))$ (4)

In Table 5, the adsorption energies (ΔGad) of LTZ on the BNNT and AlNNT nanotubes equal 14.22 and 5.80 kcal.mol-1, respectively, suggesting that placement on the AlNNT substrate is easier than placement on the

Table 4. Values of thermodynamic functions resulted from frequency calculations for LTZ drug, AlNNT nanotube, and LTZ/AlNNT mixture in gas phase.

Compounds	B3LYP/6-31G*		
	LTZ	**AlNNT**	**LTZ/AlNNT Mix**
$(G+E_{el})^a$	-927.94815	-7148.91153	-8076.85045
$(H+E_{el})^a$	-927.88026	-7148.75166	-8076.63274
$(E_{Thermal}+E_{el})^a$	-927.88120	-7148.75261	-8076.63369
$(E_0= ZPE+Eel)^a$	-927.89883	-7148.81558	-8076.71680
ZPE^a	0.247603	0.362110	0.610333
E_{el}^a	-928.14643	-7149.17769	-8077.32714
S^b	142.881	336.474	458.198

BNNT substrate. The enthalpy values (ΔHad) obtained for the placement of the LTZ drug on the BNNT and AlNNT nanotubes are 3.72 and -0.51 kcal/mol, respectively. In this context, the placement of LTZ drug is exothermic on the substrate of AlNNT nanotubes and endothermic on the substrate of BNNT nanotubes. The ΔEo and ΔEel values derived from the placement of the LTZ drug on the substrate of BNNT nanotubes were found to be equal to 3.16 and -1.50 kcal.mol-1, respectively, whereas the ΔEo and ΔEel values obtained from placing the LTZ drug on the substrate of AlNNT nanotubes were obtained to be equal to 2.71 and -1.89 kcal.mol-1, respectively. A comparison between the ΔEo and ΔEel of both BNNT and AlNNT nanotube substrates allows us to indicate that drug placement on the AlNNT substrate is exothermic. The drug-AlNNT nanotubes system has lower energy in the adsorption process and can be termed as thermodynamically advantageous. It states that there is a stronger interaction between such a drug and AlNNT than with BNNT. Hence, the drug-AlNNT nanotube system is more stable than the drug-BNNT nanotube system.

Examination of natural bonding orbitals (NBO)

Electron wave functions in NBO analysis are interpreted on the basis of the electron transfer from occupied molecular orbitals of donor Lewis structures to unoccupied molecular orbitals of acceptor Lewis structures. These new molecular orbitals are more stable than pure orbitals because the electronic wave functions are stabilized upon the creation of these orbitals. Given that the effect of non-covalent electron destabilization concerns the interaction of donor and acceptor molecular orbitals, it is, therefore, reasonable to consider charge transfer (donor-acceptor) according to generalized Lewis acid-base (20-31) theory. NBO Analysis of interactions (bonding-antibonding) at the B3LYP/6-31G* level shows that in the case of LTZ-AlNNT nanotube mixture, the highest resonance energy is due to the electron instability of LP(1)N73→BD*(2)N75-C85 (E2 = 51.96 kcal.mol-1), which is due to electron transfer from LTZ drug in LTZ-AlNNT nanotube mixture. The NBO calculations suggest that values (Fi,j) on electron instability of LP(1) N73→BD*(2)N75-C85 in LTZ-BNNT nanotube mixture are roughly equal to 0.28. This value of Fi,j (degree of orbital overlap) determined for electron transfer (Figure 2 and Table 6) shows that increased overlap reasonably explains the increase in resonance energies that come from electron instability. For LTZ drug in the absence of AlNNT nanotube, the highest amount of resonance energy was due to electron transfers of BD*(2) C15-C19→ BD*(2) C12-C17 with E2=248.23 kcal/mol, Lp(1)N1→ BD *(2) N3-C13 with E2=51.41 kcal/mol, BD (2) N3-C13→BD*(2) N2-C20 with E2=31.22 kcal/mol and Lp(1)N1→BD*(2)N2-C20 with E2 = 25.24 kcal.mol-1. When LTZ drug is placed in the presence of AlNNT nanotube, the highest amount of resonance energy was related to electron transfers of Lp(1)N73→BD*(2)N74-C92 with E2=51.96 kcal.mol-1, Lp(1)C90→BD*(3) N76-C93 with E2=37.46 kcal/mol, BD(2)N3-C13→BD*(2) N2-C20 with E2=22.31 kcal/mol, BD(2)N75-C85→ BD*(2) N74-C92 with E2=31.98 kcal.mol-1 and Lp(1)N73→BD*(2)N74-C92 with E2=25.66 kcal.mol-1 (Table 4 and Figure 3-6). The resonance energy of the LTZ-AlNNT nanotube mixture reveals that three electrons were transferred from the AlNNT nanotube to the LTZ, and one to the AlNNT nanotube from the LTZ drug. For the electrons transferring from the AlNNT nanotube to the LTZ, the following processes have been studied: BD(1) Al35-H66→ BD*(1)C78-H95 with E2=1.95 kcal/mol, BD(1)Al35-H66→BD*(1)C81-H96 with E2 =0.1

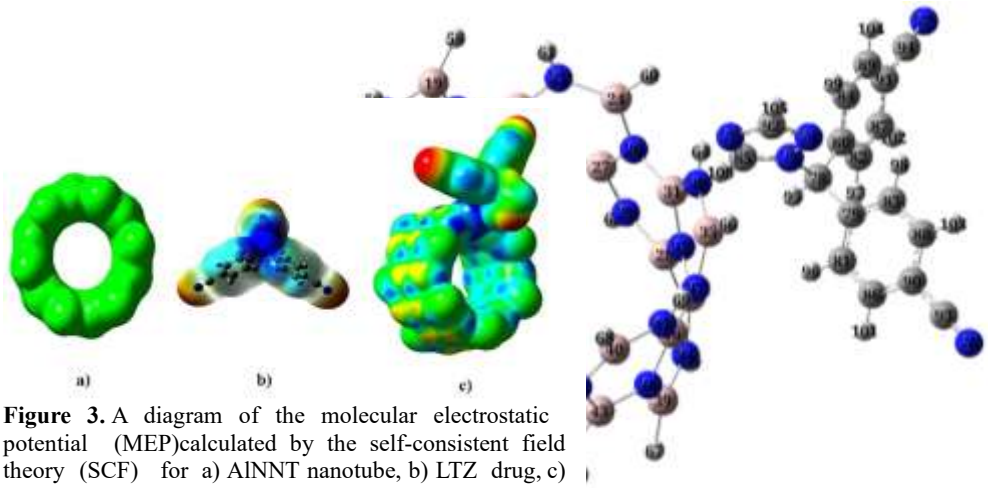

Figure 3. A diagram of the molecular electrostatic potential (MEP)calculated by the self-consistent field theory (SCF) for a) AlNNT nanotube, b) LTZ drug, c) LTZ - AlNNT nanotube complex in the ground state.

ns in the structure of Mix1 mixtures.

Table 6. Maximum resonance energies (E(2)/kcal.mol^{-1}), energy difference of orbitals (ΔE= E(j)-E(i), a.u.), the LTZ drug, LTZ - BNNT nanotube mixture using DFT calculations at the B3LYP/6-31G* level of theory.

LTZ

Donor NBO (i)	**Acceptor NBO (j)**	**E(2)**	**E(j)-E(i)**
BD (2) N 3 - C 13	BD*(2) N 2 - C 20	31.22	0.31
BD (2) C 7 - C 11	BD*(2) C16 - C 18	21.95	0.28
BD (2) C 8 - C 10	BD*(2) C15 - C 19	21.51	0.28
BD (2) C 9 - C 14	BD*(2) C 7 - C 11	20.86	0.29
BD (2) C 12 - C 17	BD*(2) C 8 - C 10	21.28	0.28
BD (2) C 16 - C 18	BD*(2) C 9 - C 14	20.11	0.28
LP (1) N 1	BD*(2) N 2 - C 20	25.24	0.28
LP (1) N 1	BD*(2) N 3 - C 13	51.41	0.27
LP (1) N 4	BD*(1) C 18 - C 21	13.08	1.02
LP (1) N 5	BD*(1) C 19 - C 22	13.09	1.02
BD*(2) C 15 - C 19	BD*(3) N 5 - C 22	19.14	0.1
BD*(2) C 15 - C 19	BD*(2) C12 - C 17	248.23	0.01

kcal/mol, BD(1)Al35-H66→ BD*(1) C85-H100 with E2=0.73 kcal/mol. The electron transfer of the LTZ drug to the AlNNT nanotube is Lp(1)C82→BD*(2) Al35-N37 with E2=0.06 kcal/mol. From the observation of the transfer of electrons, one can infer that AlNNT nanotube shows a greater conductivity than the LTZ drug, and stereo electronic interaction exists, with the LTZ drug exhibiting greater absorption characteristics compared to the AlNNT nanotube. The resonance energies of uninterrupted electron transfer by the drug molecule orbitals have changed to a considerable degree in the mixed state, as shown in Table 6. This suggests that the particular form of resonance is more strongly associated with these orbitals of the drug in pure form rather than in the mixed form. This, in turn, has diminished the aromaticity of the molecule and has diminished the resonance number. The charges on pure LTZ and LTZ in the presence of AlNNT nanotubes were calculated theoretically using B3LYP/6-31G* level of theory calculation for NBO analysis. The obtained results show the charge density changes on the atoms involved in the reaction, i.e., C11 (C83) and C12 (C84) (Table 7).

Structural parameters

The structural parameters of the LTZ drug and drug in presence of AlNNT nanotube were calculated at B3LYP/6-31G* level of theory (Tables 8 and 9). When comparing the changes of structural parameters in LTZ, AlNNT nanotube, and in combination of the two compounds, it is clear that the change in structural parameters in the interaction sites is substantially large. The received results evidently show that structural-parameter changes are directly related to the variations in resonance energies due to destabilization computed electronically. In the LTZ-AlNNT nanotube mixture, the bond length is greater than 1.466, less than 1.354, and equal to 1.528 as an average for the three different N73-C78 bond distances compared to those in the drug. The bonds are longer by approximately 0.001 angstroms with

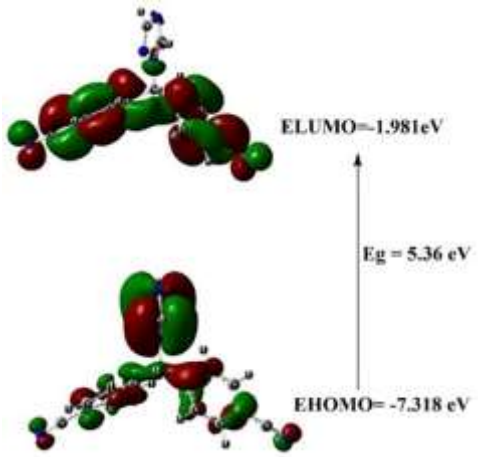

Figure 4 Molecular orbital. diagramof LTZ drug

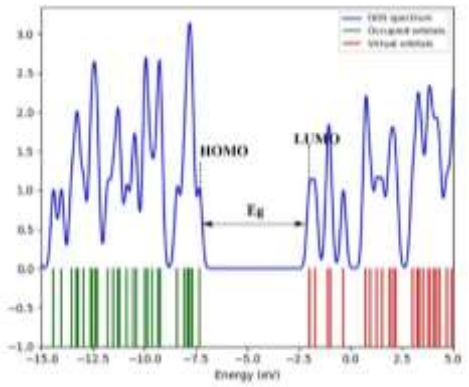

Figure 5. DOS diagram of LTZ drug .

bond lengths of rC78-C80 = 1.530, rC90-C91 = 1.379, rC79-C83 = 1.401, and rC86-C90 = 1.403 compared to their respective lengths in the drug. The bonds are shorter by 0.002 Å in the LTZ-AlNNT nanotube complex with a bond length of 1.404 (C80-C82) as compared to the same bond in the drug alone, thus the bonding variations of the present drug with respect to the nanotube have suffered the greatest change of 0.005 Å in comparison with the other ones. The bond length changes recorded in the drug-nanotube mixture and drug alone, as shown in the table, are not perceptible, with changes to bond length less than 0.005 A˚. In the table due to the changes of bond angles (Table 9), in the mixture of LTZ- AlNNT nanotube, the bond angles are A N73-C78-C79=3.111, AC78-C79-C83=4.121 and A C78- C80-C82=6.117 increased with AN1-C6-C7=113.4, AC6-C7-C11= 2.123and A C6-C8-C10 =5.119, respectively, in the drug.

In the table due to the changes of bond angles (Table 9), in LTZ- AlNNT nanotube drug mixture, the bond angles are A N73-C78-C80=5.113, AC78-C79-C81=4.119 and A C78- C80-C84 =3.123 is shortened by A N1-C6-C8=111/1, A C6-C7-C9=117/8, and A C6-C8-C12=121/3, respectively, compared to these angles.

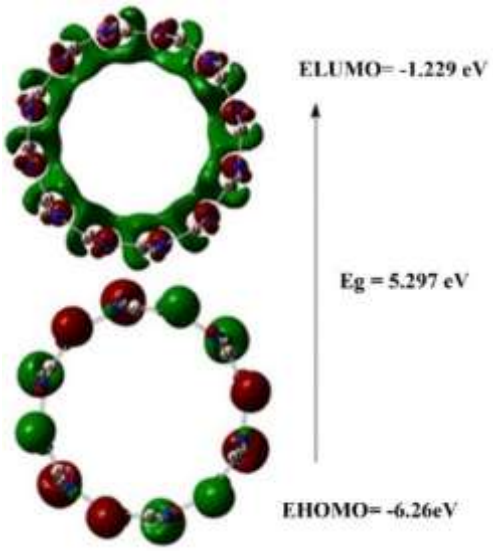

Figure 6. Diagram of molecular orbital of AlNNT nanotube.

Table 7. Charge distribution calculated by NBO for alone LTZ drug and LTZ in the presence of AlNNT nanotubes using calculations at B3LYP/6-31G* level of theory.

Natural charge				
Within (Drug)		**Within (Drug) in Drug-AlNNT**		Δ(q)
N 1	-0.21095	N 73	-0.21032	0.001
N 2	-0.32984	N 74	-0.33195	0.002
N 3	-0.50627	N 75	-0.5092	0.003
N 4	-0.29554	N 76	-0.29699	0.001
N 5	-0.29447	N 77	-0.29838	0.004
C 6	-0.06841	C 78	-0.07333	0.005
C 7	-0.03229	C 79	-0.03128	0.001
C 8	-0.03202	C 80	-0.02857	0.003
C 9	-0.22126	C 81	-0.22233	0.001
C 10	-0.22076	C 82	-0.22323	0.002
C 11	-0.22627	C 83	-0.20213	0.024
C 12	-0.20106	C 84	-0.22496	0.024
C 13	0.19614	C 85	0.19739	0.001
C 14	-0.17732	C 86	-0.17945	0.002
C 15	-0.1787	C 87	-0.17794	0.001
C 16	-0.17298	C 88	-0.1777	0.005

Table 8. Values of the optimized bonds length of the LTZ drug alone and in the presence of AlNNT nanotubes.

Optimized structure parameters / B3LYP/6-31G*

Within (Drug) in AlNNT- Drug		**Within (Drug)**		**Δr**
Bonds	**Bond lengths (Å)**	**Bond**	**Bond lengths (Å)**	
(N73-C78)	1.466	(N1-C6)	1.467	-0.001
(N73-C85)	1.354	(N1-C13)	1.355	-0.001
(C78-C79)	1.528	R(C6-C7)	1.529	-0.001
(C78-C80)	1.53	R(C6-C8)	1.528	0.002
(C79-C81)	1.399	R(C7-C9)	1.403	-0.004
(C79-c83)	1.401	(C7-C11)	1.399	0.002
(C80-C82)	1.404	(C8-C10)	1.399	0.005
(C80-C84)	1.399	(C8-C12)	1.401	-0.002
(C81-c86)	1.392	(C9-C14)	1.389	0.003
(C82-C87)	1.389	(C10-C15)	1.392	-0.003
(C83-88)	1.39	(C11-C16)	1.394	-0.004
(C84-C89)	1.394	(C12-C17)	1.39	0.004
(C86-C90)	1.403	(C14-C18)	1.405	-0.002
(C87-C91)	1.406	(C15-C19)	1.403	0.003
(C88-C90)	1.406	(C16-C18)	1.403	0.003
(C89-C91)	1.402	(C17-C19)	1.406	-0.004

Table 9. Values of optimized bond angles of LTZ drug alone and in the presence of AlNNT nanotube.

Optimized structure parameters / B3LYP/6-31G*

Within (Drug)		**Within (Drug) in AlNNT- Drug**		**Δθ**
Atoms	**Bond angle (°)**	**Atoms**	**Bond angle (°)**	
(N74-N73-C78)	122.5	(N2-N1-C6)	122.3	0.2
N(74-N73-C85)	109.4	(N2-N1-C13)	109.3	0.1
(C78-N73-C85)	128	(C6-N1-C13)	128.4	-0.4
(N73-C78-C79)	111.3	(N1-C6-C7)	113.4	-2.1
(N73-C78-C80)	113.5	(N1-C6-C8)	111.1	2.4
(N73-C78-C95)	104	(N1-C6-C23)	104.2	-0.2
(N73-C85-N75)	110.6	(N1-C13-N3)	110.7	-0.1
(N73-C85-C100)	122.7	(N1-C13-C28)	123	-0.3

Hence, according to the findings derived from the NBO analysis, it can be conferred that modifications in structural parameters could be one of the methods through which the drug-aluminum nitride nanotube interaction can be elucidated based on electronic transfers (stereo electronic effects) that occur across the

two systems involved in the reaction.

Electrostatic potential

Determining the molecular electrostatic potential is one of the several important characteristics that can be studied with regard to the reactivity. MEP indicates a red site as the site of most negative charge, which would be expected to act as the site for electrophile molecule attack, whereas the site of maximum positive charge is blue-represented and can be expected to function as a possible site for nucleophile molecule attack. The most important aspect of MEP is that one can create a construct to illustrate the size of the molecule using centers of negative and positive electrostatic potential as well as a color range similar to molecular shapes. Generally, MEP determines nucleophilic and electrophilic sites in a molecule and predicts active sites to participate in the reaction. From the pertinent depiction, it becomes apparent that when the LTZ drug is placed alone, in the absence of the AlNNT nanotube, the nucleophilic and electrophilic centers are clearly visible in blue and red colors. When the LTZ drug is laid over the surface of the AlNNT nanotube, all the nucleophilic and electrophilic centers of LTZ are neutralized. It can therefore be concluded that LTZ interacts with the AlNNT nanotube (Figure 3). As for HOMO-LUMO analysis, it was found by DFT: B3LYP calculations that the energy gap in the mixture of drug and AlNNT nanotube (4.756 eV) is appreciably much less than the energy gap in the drug molecule (Eg=336.5 eV) and that in the AlNNT nanotube (Eg=336.5 eV) (Figures 4-8). In other words, the reactivity of a molecule is inversely related to its energy gap (32-38). Hence, the result indicates that drug loading on the nanotube surface may soften the drug, impart conductivity, and greatly enhance its reactivity. The energy gap of the molecular orbitals (E LUMO - E HOMO) also provides information regarding the stabilizing orbital interactions where further decrease in energy level of the electron acceptor orbital (LUMO energy level) and increase in energy level of electron donor orbital (HOMO energy level) gives rise to enhanced energy difference resulting in the destabilization of electrons hence confirming change in the electron population in electron donor and acceptor orbital combinations. At a close read of the table of reactivity indices parameter in the LTZ-AlNNT nanotubes blend, decrease in energy gap brings with it an increase in the softness parameter while the hardness parameter decreases by a small margin with decreases in ionization energy and electron affinity, in addition to decreases in the electronegativity and electrophilicity values. Thus, the aforementioned changes associated with the reactivity index can be accounted for by taking into consideration the electron-withdrawing effects of the two nitrile groups and the electron-donating resonance

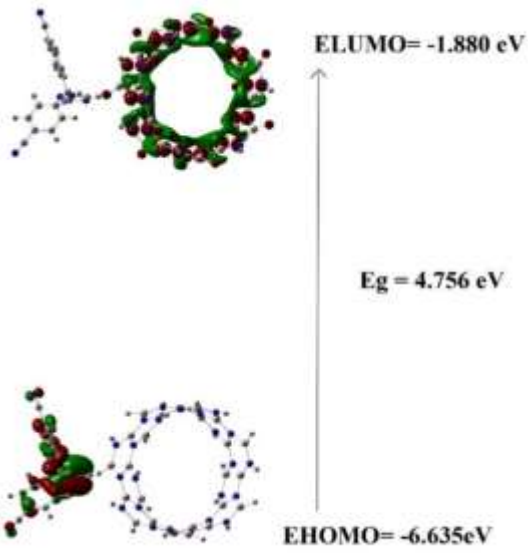

Figure 7. Molecular orbital diagram of LTZAlNNT mixtur.

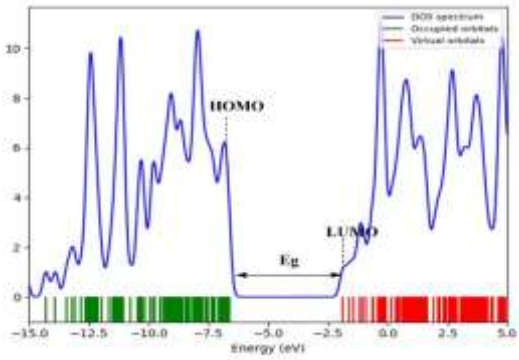

Figure 8. -DOS diagram of LTZAlNNT mixture

effects of the aromatic rings in the AlNNT nanotubes/letrozole drug system. Adsorption of the LTZ drug onto the surfaces of this AlNNT nanotube system showed the dual effects of the electron-donating aromatic rings and the electron-withdrawing nitrile, which account for such changes. Figures 4 to 8 showing the energy gap time between HOMO-LUMO molecular orbitals and DOS diagrams employed to assess the shape of molecular orbitals of drug LTZ, it appears that the HOMO orbital is localized on the imidazolium substituent and across a number of double bonds in the aromatic ring while the LUMO orbital is on the aromatic rings and two nitrile groups. By this, it can be inferred that one can predict the possibility of reaction with electrophilic species in the region where HOMO orbitals are relatively more distributed and to nucleophilic species in the region where LUMO orbitals are concentrated (28-31).

Concentrations of LUMO and HOMO orbitals across regions of AlNNT nanotube-shaped molecular orbitals are such that LUMO orbitals are more confined to the inside of the ring and HOMO orbitals are more dispersed outside the ring and on the nanotube ring. The study of the geometry of molecular orbitals in the LTZ-AlNNT nanotube mixture reveals that the HOMO orbitals are more distributed on the LTZ drug, while the LUMO orbital is spread on the AlNNT nanotube, hence indicating a satisfactory interaction between the drug and the nanotube (Figures 4-8).

UV-Vis spectra analysis

The theoretical UV-Vis absorption of LTZ drug and its mixture with AlNNT was obtained using the TD-DFT method, and the key results are summarized in Table 10. The λmax values for LTZ and their mixture are observed in the UV range. The λmax of LTZ is recorded at 226.7 nm, corresponding to the excited state transition $S_0 \rightarrow S_{10}$, with contributions from H-5 → L (29%), H-4 → L+1 (-27%), H-3 → L+3 (5%), H-3 → L (23%), H-3 → L (21%), H-2 → L (35%), H-1 → L (25%), and H → L (11%). After the adsorption of the LTZ drug on the BNNT, λmax appear at 281.1 nm (f = 0.031). The charge transfer at λmax = 281.1nm is related to the excited state S0 →S12 and is defined by four configurations including (H-2→L+3 (10%), H→L+2 (39%), H→L+3 (46%), H→L+4 (31%)). The major contribution to the absorption maxima related to HOMO→LUMO + 3 (H→L + 3), which contributes about 46% of the total excitations. Upon interaction with an AlNNT nanotube, the λmax of the LTZ- AlNNT mixture increases to 254.3 nm (redshift), corresponding to the $S_0 \rightarrow S_{20}$ excited state transition. The significant transitions at λmax = 254.3 nm include H-23 → L (-14%), H-20 → L+1 (12%), H-18 → L (13%), H-18 → L+1 (-12%), H-17 → L+1 (12%), H-10 → L (61%), and H-10 → L+5 (15%). The major contribution to the absorption greatest related to HOMO-10→LUMO (H-10 → L), which contributes about 61% of the total excitations. The other excited states of the title compound are very small in intensity (f ≈ 0) and are almost forbidden due to considerations of orbital symmetry. The results indicate that an interaction occurs between LTZ and AlNNT, causing a redshift and increasing λmax from 226.7 to 254.3 nm. The UV spectra of the studied compounds are presented in Figures 9 through 11.

IR Spectrum of LTZ

At 841 cm^{-1} and 899 cm^{-1}, weak absorption bands were attributed to the out-of-plane bending vibrations of the N1=C13-H28 and N2=C20-H33 bonds, respectively. Another sharp strong band appears at 1558 cm^{-1}, which corresponds to the frequency of symmetric and asymmetric bending vibrations of the N2=C20 and N3=C13 bonds in the imidazole ring. The band at 1467 cm^{-1} is attributed to the in-plane stretching vibrational mode of the C13-N1, along with the bending C-H

Table 10. Significant results of UV-Vis absorption of LTZ drug, LTZ-AlNNT Mix and LTZ-AlNNT Mix systems.

System	Excited State	Wavelength (nm)	Excitation Energy (eV)	State assignments	Oscillator Strength (f)
LTZ	$S_0 \rightarrow S_{10}$	226.7	5.47	H-2⟶L (35%)	0.207
LTZ-AlNNT Mix	$S_0 \rightarrow S_{20}$	254.3	4.87	H-10⟶L (61%)	0.176
LTZ-BNNT Mix	$S_0 \rightarrow S_{12}$	281.1	4.41	H⟶L+3 (46%)	0.031

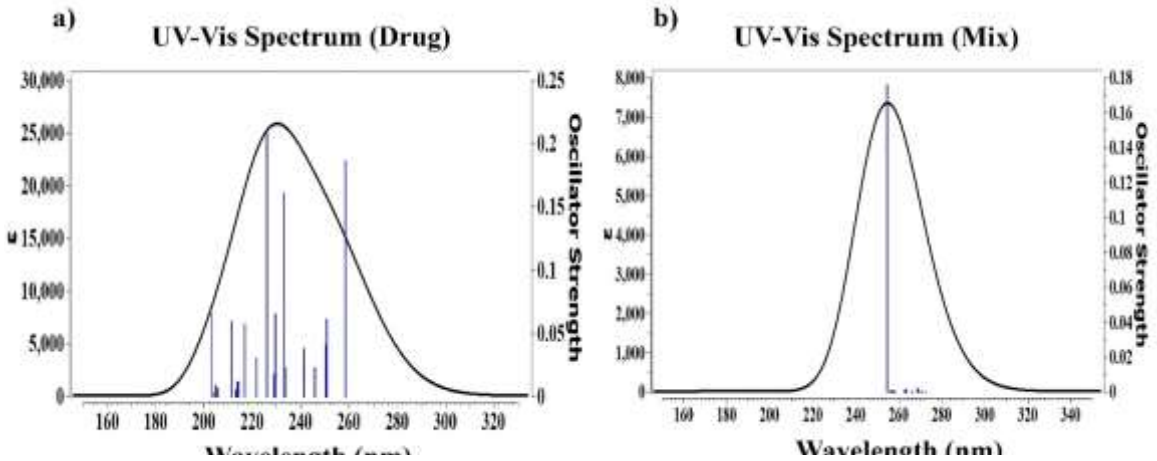

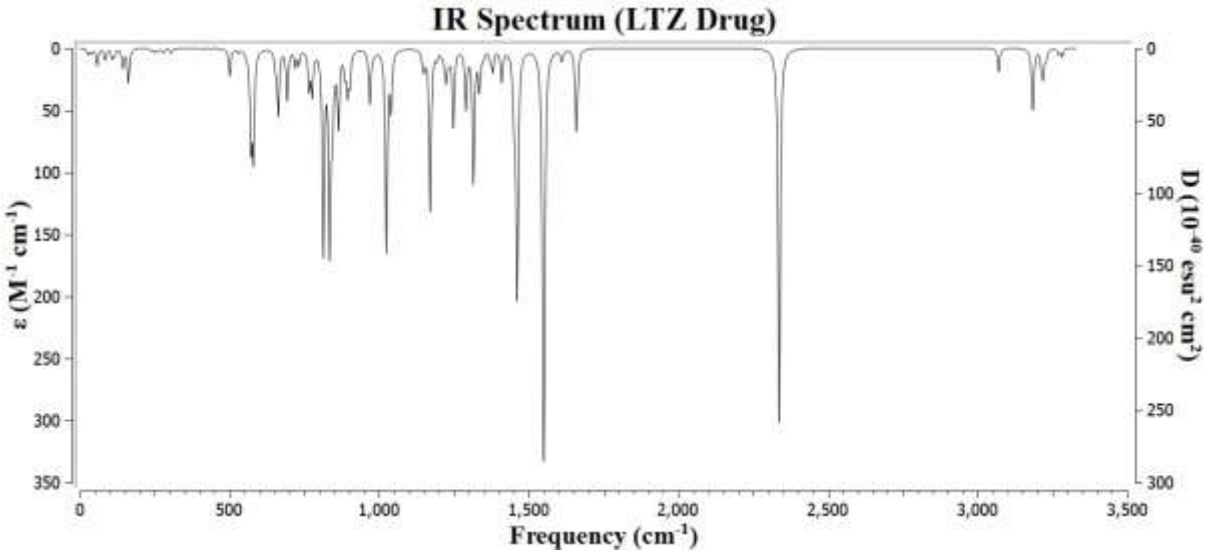

Figure 12. IR spectrum of LTZ drug using the B3LYP/6-31G* level of theory.

Table 11. Comparison of frequency changes between LTZ drug, AlNNT nanotube, and the LTZ-AlNNT mixture.

Frequencies of absorption bands in the IR spectrum (cm^{-1})

AlNNT Nanotube	LTZ-AlNNT Mix	Δ υ (LTZ-AlNNT Mix)	LTZ	LTZ-AlNNT Mix	Δ υ (LTZ-AlNNT Mix)
564	564	0.0	2350	2349	1.0
915	917	2.0	1558	1558	0.0
955	955	0.0	1467	1474	2.0

vibration of the imidazole ring of letrozole and appears with very strong intensity. A medium-intensity peak appearing at 1027 cm^{-1} is associated with the asymmetric bending vibration of N1-N2. Moreover, the extremely strong absorption bands at 1174 cm^{-1} and 1317 cm^{-1} correspond to the asymmetric bending vibrations of N=C-H. The absorption bands at 818 cm^{-1} and 836 cm^{-1} correspond to the symmetric out-of-plane bending vibrations of C-H in the aromatic rings of letrozole. The medium-intensity peak at 2350 cm^{-1} corresponds to the symmetric stretching vibration of the nitrile group attached to the aromatic ring of letrozole. In addition, weak peaks appearing at around 3233, 3236, and 3281 cm^{-1} are attributed to the C-H stretching vibrations from the imidazole ring. The experimental FT-IR spectrum has assigned the region of 3045 cm^{-1} to =C-H stretching frequency. The stretching frequency of the nitrile group appears at 2220 cm^{-1}, while out-of-plane C-H stretching frequencies appear in the regions of 690 cm^{-1} and 900 cm^{-1}.It is interesting that upon comparing the IR spectra obtained from the B3LYP/6-31G* level of theory with the experimental spectrum, it is noticeable that the results come close to each other and confirm each other (Figure 12 and Table 11).

IR Spectrum of AlNNT nanotube

In the region near 564 cm^{-1}, the bending vibration frequencies of the N-H bonds are found with medium intensity. The region near 915 cm^{-1} corresponds to strong and sharp absorption of asymmetric stretching vibrations of the Al-N-Al bond. The sharp peak at 955 cm^{-1} is due to Al-N stretching vibrations in addition to bending vibrations of N-H bonds. In the 1029 cm^{-1} region, the bending vibration of N-H bonds presents as a weak absorption band. The asymmetric stretching vibration frequencies of the Al-H bonds are observed in the 1931 cm^{-1} region. As observed in the IR spectrum, the largest vibrations in the LTZ-AlNNT Mix correspond to the N−H bending vibration and the Al−N stretching vibration, which occur at 955 cm^{-1}. The presence or absence of the drug on the nanotube substrate does not significantly change this frequency. N−H bending vibrations show medium intensity between 1032 cm^{-1}.

This vibration most likely shifts when considering the nanotube in the absence of the drug compared to when presence of letrozole because of interactions occurring

between the nanotube and the drug. In the 1932 cm^{-1} region appears another absorption band corresponding to the asymmetric stretching vibrations of Al−H bonds, which have not significantly changed with respect to that of the pure AlNNT nanotube (Figure 13 and Table 11).

IR Spectrum of the LTZ–AlNNT Mix

It is noteworthy that the absorption frequencies at 2350 cm^{-1}, 1467 cm^{-1}, and 1027 cm^{-1}, which belong to the drug alone, shift to 2349 cm^{-1}, 1474 cm^{-1}, and 1028 cm^{-1}, respectively, when the drug is placed on the nanotube substrate. This shows changes in the vibrational frequencies of the nitrile group (stretching vibration), C=N bond (stretching vibration), and C=N-H bond (bending vibration). So, it can be concluded that there is interaction between the AlNNT nanotube and the drug LTZ (Figure 14 and Table 11).

The non-covalent interaction index (NCI)

By examining the noncovalent interaction index (NCI) parameter, one could see whether these interactions between AlNNT nanotube and LTZ drug were noncovalent and how they were measured in terms of the number and type of intermolecular interactions. NCI is given by Eq. 10 (39-43):

$$RDG(r) = \frac{1}{2(3\pi^2)^{1/3}} \frac{|\nabla\rho(r)|}{\rho(r)^{4/3}} \quad \text{(Eq.10)}$$

The RDG distribution versus the electron density ρ and sign λ2 is plotted in Figure 15. On the plot, X-axis values show sign values $\lambda_2\rho(r)$ and Y-axis values show corresponding RDG values. Values for $\lambda_2\rho(r)$ and NCI-RDG were analyzed with the Multiwfn program. In the RDG scatter plot, very weak van der Waals interactions and repulsive-space interactions are painted green and red respectively, representing regions of low electron

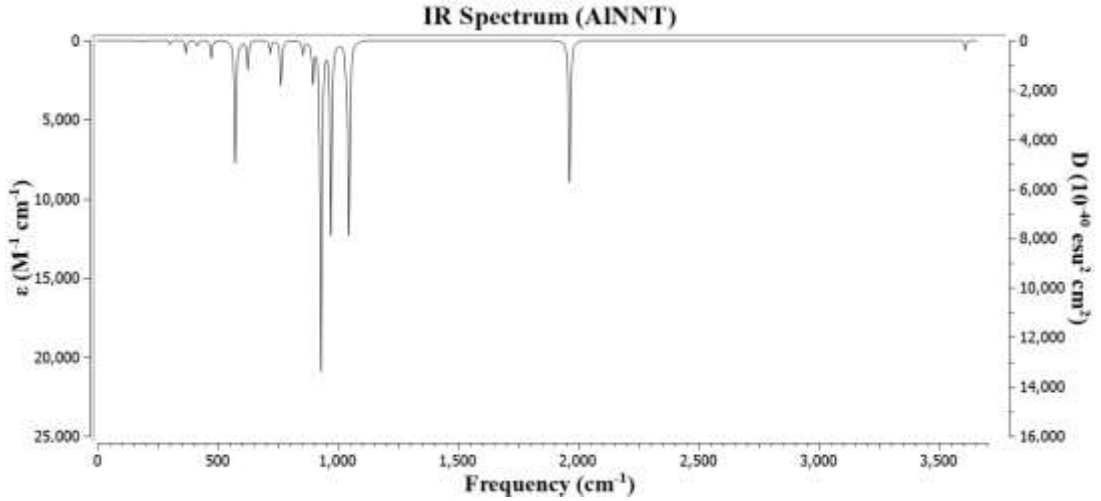

Figure 13. IR spectrum of AlNNT using the B3LYP/6-31G* level of theory.

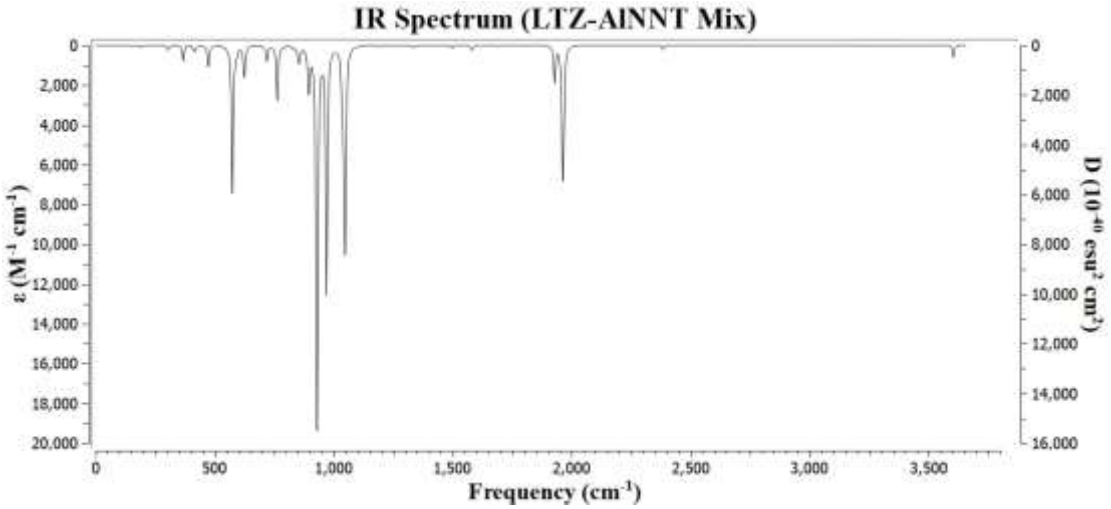

Figure 14. IR spectrum of LTZ - AlNNT Mix using the B3LYP/6-31G* level of theory.

density. At the critical points, the density gradient values also observe while weak interactions exist giving rise to peaks in the NCI plot. Negative blue was set up to show RDG scatter dots in H-bonding interactions (44-45). The NCI diagram of the LTZ/AlNNT complex clearly shows the weak interaction of the AlNNT nanotube with the LTZ drug (Figure 15). In the case of the NCI diagram of the LTZ/AlNNT complex, Figure 15 proves the weak interaction between the AlNNT nanotube and the LTZ drug. Also, red and green regions or colors are found in NCI diagrams. Some are formed between the nitrogen atom of the triazole ring of LTZ drug and the aluminum atom of the nanotube, which is consistent with these weak interactions and steric effect shown in Figures 15 and 16. The results indicate that the intermolecular interactions provided are through the drug atoms and the nanotube that could be of the van der Waals variety and identified the steric effect between the negatively charged nitrogen atom of the triazole ring of the LTZ drug and the positively charged hydrogen atoms of the nanotube. For the LTZ drug, the green areas represent regions where more interferences are introduced due to accommodation of LTZ drug into the nanocavities. Steric spaces account for more than what was seen in red. The red and green spots on the nanotube surface arise due to the repulsive and steric effect of the rings that make up the quantum dot structure. This has been confirmed with red and green spikes observed on the scatter map of 2D-RDG for all the considered LTZ/AlNNT complexes shown in Figure 15.

The scatter plot in Figure 15 shows many spikes in an area from -0.05 to +0.05 a.u. Moreover, negative values of sign(λ2)ρ (blue side of Figure 6) are indicating attractive interactions with another molecule, whereas

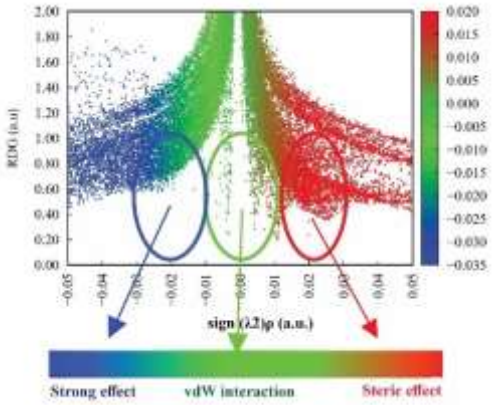

Figure 15. Pictographic depiction of the non-covalent interaction analysis (2D).

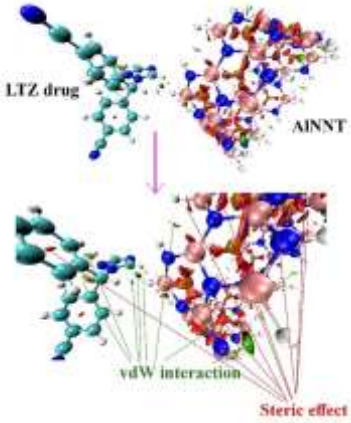

Figure 16. Pictographic depiction of the non-covalent interaction analysis (3D).

positive values of sign(λ2)ρ (red side of Figure 15) are denoting high repulsion interactions (steric effect). As discerned from Figure 15, the range of values of sign(λ2)ρ between -0.01 and +0.01 concurs with van der Waals forces exerted in low distribution, whereas the range between +0.01 and +0.02 is for steric effects and the range between -0.01 and -0.02 is for vdW interaction. From Figure 16, it can be observed that the distribution of steric effects is almost identical to strongest interaction.

Conclusion

In this research, an investigation has been conducted theoretically with respect to the interaction of the LTZ drug with the BNNT and AlNNT nanotubes. The DFT calculations at the B3LYP/6-31G* level of theory and NBO analysis were performed. The outcome of this investigation is the structural features for bonding thermodynamic parameters such as stereoelectronic interactions, electrostatic interactions, and the reactivity level of LTZ drug in the presence of two nanotubes. Adsorption of LTZ onto the BNNT and AlNNT microtubes indicates ΔGad values of 14.22 and 5.80 kcal.mol-1 respectively, which is presented as an easier process for adsorption in AlNNT. The ΔHad values are therefore exothermic for AlNNT at 3.72 kcal. mol-1 and endothermic for BNNT at -0.51 kcal.mol-1. The comparison between ΔE0 and ΔEel clearly indicates that adsorption on the AlNNT is thermodynamically favorable because of the larger strength of interaction and increased stability offered as compared to BNNT. According to the results of thermochemical parameters obtained in loading LTZ drug on the substrate of BNNT and AlNNT nanotubes (6,6), the interaction of the LTZ with AlNNT nanotube is a more spontaneous and exothermic process than its interaction with the BNNT nanotube. The results from calculation of the dipole moment show that the drug is an electron-rich polar molecule and the nanotube is an electron-deficient non-polar molecular structure.

So, the interaction here is in charge transfer form, and it is supported also by resonance energies among the two LTZ-AlNNT nanotube mixtures, for the fact that the interaction is probably formed by Van der Waals

interaction between these two components. The incorporation of the LTZ drug on the AlNNT enhances the wavelength at which the maximum absorption occurs from 226.7 to 254.3 nm, and the incorporation of the LTZ drug to the BNNT increases the wavelength of maximum absorption from 226.7 to 281.1 nm, thus the changes can be considered as a bathochromic effect (redshift).We hope our findings about the adsorption properties of LTZ by BNNT and AlNNT nanotubes can help improve the delivery of sorbent-enhancing drugs to cancer cells, thereby minimizing drug interactions with healthy tissues.

Acknowledgement

The authors gratefully acknowledge from the Islamic Azad University, Roudehen and Central Tehran Branches, Iran.

References

1. Ziani K, Fang Y, McClements DJ. Encapsulation of functional lipophilic components in surfactant-based colloidal delivery systems: Vitamin E, vitamin D, and lemon oil. Food chemistry. 2012 Sep 15;134(2):1106-12.
2. Elhissi A, Ahmed W, Dhanak V, Subramani K. Carbon nanotubes in cancer therapy and drug delivery. InEmerging nanotechnologies in dentistry 2012 Jan 1 (pp. 347-363). William Andrew Publishing.
3. Vashist SK, Zheng D, Pastorin G, Al-Rubeaan K, Luong JH, Sheu FS. Delivery of drugs and biomolecules using carbon nanotubes. Carbon. 2011 Nov 1;49(13):4077-97.
4. Mendes RG, Bachmatiuk A, Büchner B, Cuniberti G, Rümmeli MH. Carbon nanostructures as multi-functional drug delivery platforms. Journal of Materials Chemistry B. 2013;1(4):401-28.
5. Mendes RG, Bachmatiuk A, Büchner B, Cuniberti G, Rümmeli MH. Carbon nanostructures as multi-functional drug delivery platforms. Journal of Materials Chemistry B. 2013;1(4):401-28.
6. Lin Y, Bunker CE, Fernando KS, Connell JW. Aqueously dispersed silver nanoparticle-decorated boron nitride nanosheets for reusable, thermal oxidation-resistant surface enhanced Raman spectroscopy (SERS) devices. ACS applied materials & interfaces. 2012 Feb 22;4(2):1110-7.
7. Griebel M, Hamaekers J. Molecular dynamics simulations of boron-nitride nanotubes embedded in amorphous Si-BN. Computational materials science. 2007 May 1;39(3):502-17.
8. Hughes GA. Nanostructure-mediated drug delivery. Nanomedicine: nanotechnology, biology and medicine. 2005 Mar 1;1(1):22-30.
9. Yang L, Sheldon BW, Webster TJ. Nanophase ceramics for improved drug delivery. Am Ceram Soc Bull. 2010;89(2):24-32.
10. El Khalifi M, Duverger E, Gharbi T, Boulahdour H, Picaud F. Theoretical demonstration of the potentiality of boron nitride nanotubes to encapsulate anticancer molecule. Physical Chemistry Chemical Physics. 2015;17(44):30057-64.
11. Shakerzadeh E, Noorizadeh S. A first principles study of pristine and Al-doped boron nitride nanotubes interacting with platinum-based anticancer drugs. Physica E: Low-dimensional Systems and Nanostructures. 2014 Mar 1; 57:47-55.
12. Frisch MJ, Trucks GW, Schlegel HB, Scuseria GE, Robb MA, Cheeseman JR, Montgomery Jr JA, Vreven T, Kudin KN, Burant JC, Millam JM. Gaussian 03, Revision D. 01, 2004, Gaussian, Inc. Wallingford, CT.
13. Lewars E. Introduction to the theory and applications of molecular and quantum mechanics. J. Computational chemistry, Ontario Canada. 2003.
14. Jalali Sarvestani MR, Ahmadi R. Evaluating the Performance of 2, 3-dihydro-1H-phenothiazine-4 (5aH)-one as an Ionophore in Construction of a Cation Selective Electrode by Density Functional Theory. International Journal of New Chemistry. 2018 Jan 1;5(1):1-0.
15. Jalali Sarvestani MR, Ahmadi R. Investigating the Complexation of a recently synthesized phenothiazine with Different Metals by Density Functional Theory. International Journal of New Chemistry. 2017 Dec 1;4(4):101-10.
16. Masnabadi N. DFT Study and NBO analysis of conformation properties of 2, 5, 5-Trimethyl-1, 3, 2-Dioxaphosphinane 2-selenide and their dithia and diselena analogous. Journal of Sciences, Islamic Republic of Iran. 2020 Apr 1;31(2):137-46.
17. Danaie E, Masoudi S, Masnabadi N. A Computational Study of the Conformational Behavior of 2, 5-Dimethyl-1, 4-dithiane-2, 5-diol and Analogous S and Se: DFT and NBO Study. Letters in Organic Chemistry. 2020 Oct 1;17(10):749-59.
18. Masnabadi N. The study of Letrozole adsorption upon CCT nanotube: A DFT/TD-DFT and spectroscopic (excited states and UV/Vis). Main Group Chemistry. 2022 Dec 20;21(4): 1013-27.doi:10.3233/MGC-210098
19. Hosseinzadeh M, Masoudi S, Masnabadi N, Azarakhshi F. Adsorption of Diethylstilbestrol Drug into BNNT: DFT/TD-DFT and Spectroscopic (Excited States, UV/Vis and NMR) Studies. Letters in Organic Chemistry. 2023 Apr 1;20(4):347-61.
20. Glendening ED, Badenhoop JK, Reed AE, Carpenter JE, Bohmann JA, Morales CM, Landis CR, Weinhold F. NBO 6.0. Theoretical Chemistry Institute, University of Wisconsin, Madison. 2013.
21. Politzer P, Seminario JM, editors. Modern density functional theory: a tool for chemistry. Elsevier; 1995 Jan 27.
22. Masnabadi N. DFT and NBO analysis on conformers of dioxaphosphinane derivatives. Int. J. Bio-Inorg. Hybr. Nanomater. 2022;11(3):127-35.
23. Masnabadi N. Conformational Stability, FMO, NMR, MEP and NBO Analysis of 2, 5-Dimethyl-2, 5-bis (methylthio)-1, 4-dithiane and Dimethoxy compounds by DFT Approach. Letters in Organic Chemistry. 2021 Aug 1;18(8):656-68.
24. Masnabadi N, Thalji MR, Alhasan HS, Mahmoodi Z, Soldatov AV, Ali GA. Structural, electronic, reactivity, and conformational features of 2, 5, 5-trimethyl-1, 3, 2-diheterophosphinane-2-sulfide, and its derivatives: DFT,

MEP, and NBO calculations. Molecules. 2022 Jun 22;27(13):4011.
25. Mikołajczyk M, Ziemnicka B, Krzywański J, Cypryk M, Gostyński B. Nucleophilic substitution at tetracoordinate phosphorus. stereochemical course and mechanisms of nucleophilic displacement reactions at phosphorus in diastereomeric cis-and trans-2-halogeno-4-methyl-1, 3, 2-dioxaphosphorinan -2-thiones: Experimental and DFT studies. Molecules. 2021 Jun 15;26(12):3655.
26. Doust Mohammadi M, Abdullah HY. The adsorption of chlorofluoromethane on pristine, Al-, Ga-, P-, and As-doped boron nitride nanotubes: a PBC-DFT, NBO, and QTAIM study. ChemistrySelect. 2020 Oct 22;5(39):12115-24.
27. Sakr MA, Sherbiny FF, El-Etrawy AA. Hydrazone-based materials; DFT, TD-DFT, NBO analysis, fukui function, MESP analysis, and solar cell applications. Journal of Fluorescence. 2022 Sep;32(5):1857-71.
28. Sindhuja S, Karnan M, Gayathri R, Kavimani M. Non-covalent interaction, topology, molecular properties, spectral and quantum chemical analysis of 2, 5-dinitrophenol. Journal of the Indian Chemical Society. 2024 Oct 1;101(10):101276.
29. Liu XM, Zhao DX, Yang ZZ. Transition from Noncovalent Interaction to Covalent Bond Based on One-Electron Potential, Quantum Chemical Topology, and Molecular Face Theory. The Journal of Physical Chemistry A. 2025 Jun 30.
30. Goswami S, Ganguly A. Analysis of Non-Covalent Interactions Present within a Series of Nucleobase Dimers from the Perspective of Quantum Topology and Aromaticity. Advanced Theory and Simulations. 2025 Apr 22:2500121.
31. Tretiakov S, Nigam A, Pollice R. Studying Noncovalent Interactions in Molecular Systems with Machine Learning. Chemical reviews. 2025 Jun 9.
32. Sharma SK, Chiang LY, Hamblin MR. Photodynamic therapy with fullerenes in vivo: reality or a dream? Nanomedicine. 2011 Dec 1;6(10):1813-25. https://doi.org/10.2217/nnm.11.144
33. Faver JC, Zheng Z, Merz KM. Model for the fast estimation of basis set superposition error in biomolecular systems. The Journal of chemical physics. 2011 Oct 14;135(14). https://doi.org/10.1063/1.3641894
34. Sahayarayan JJ, Rajan KS, Vidhyavathi R, Nachiappan M, Prabhu D, Alfarraj S, Arokiyaraj S, Daniel AN. In-silico protein-ligand docking studies against the estrogen protein of breast cancer using pharmacophore based virtual screening approaches. Saudi Journal of Biological Sciences. 2021 Jan 1;28(1):400-7.
35. Luo J, Zhang R, Wang X, Hou Z, Guo S, Jiang B. Binding properties of marine bromophenols with human protein tyrosine phosphatase 1B: Molecular docking, surface plasmon resonance and cellular insulin resistance study. International Journal of Biological Macromolecules. 2020 Nov 15; 163:200-8.
36. Paneru TR, Chaudhary MK, Tandon P, Chaudhary T, Joshi BD. Theoretical study on molecular stability, reactivity, and drug potential of cirsilineol from DFT and molecular docking methods. Chemical Physics Impact. 2024 Jun 1; 8:100641.
37. Adindu EA, Godfrey OC, Agwupuye EI, Ekpong BO, Agurokpon DC, Ogbodo SE, Benjamin I, Louis H. Structural analysis, reactivity descriptors (HOMO-LUMO, ELF, NBO), effect of polar (DMSO, EtOH, H2O) solvation, and libido-enhancing potential of resveratrol by molecular docking. Chemical Physics Impact. 2023 Dec 1; 7:100296.
38. Zhang S, Zhao D, Cui Q. Gap-Δenergy, a New Metric of the Bond Energy State, Assisting to Predict Molecular Toxicity. ACS omega. 2024 Apr 12;9(16):17839-47.
39. Sarala S, Geetha SK, Muthu S, Irfan A. Computational investigation, comparative approaches, molecular structural, vibrational spectral, non-covalent interaction (NCI), and electron excitations analysis of benzodiazepine derivatives. Journal of Molecular Modeling. 2021 Sep;27(9):266.
40. Kříž K, Řezáč J. Non-covalent interactions atlas benchmark data sets 4: σ-hole interactions. Physical Chemistry Chemical Physics. 2022;24(24):14794-804.
41. Sunny SA, Thomas R. Exploring non-covalent interactions: A computational study of Methyl acetate in chloroform and Hexafluoroisopropanol. Chemical Physics Impact. 2024 Jun 1; 8:100514.
42. Kumar AR, Ilavarasan L, Mol GS, Selvaraj S, Azam M, Jayaprakash P, Kesavan M, Alam M, Dhanalakshmi J, Al-Resayes SI, Ravi A. Spectroscopic (FT-IR, FT-Raman, UV–Vis and NMR) and computational (DFT, MESP, NBO, NCI, LOL, ELF, RDG and QTAIM) profiling of 5 chloro-2 hydroxy-3-methoxybenzaldehyde: a promising antitumor agent. Journal of Molecular Structure. 2024 Feb 15; 1298:136974.
43. Neetha S, Santhosh C, Sheela K, Ravi Singh K, Sridhar M, Sadashiva M. A comprehensive analysis of the molecular packing in the crystal of (4-methoxyphenyl) methyl 4-(4-chlorophenyl)-1, 3-thiazole-2-carboxylate: insights of X-ray crystallography and DFT analysis. Journal of Molecular Structure. 2025 Jan 5; 1319:139584.
44. Jia Z, Pang H, Li H, Wang X. A density functional theory study on complexation processes and intermolecular interactions of triptycene-derived oxacalixarenes. Theoretical Chemistry Accounts. 2019 Sep;138(9):113.
45. Glendening ED, Landis CR, Weinhold F. NBO 7.0: New vistas in localized and delocalized chemical bonding theory. Journal of computational chemistry. 2019 Sep 30;40(25):2234-41.